REPORT DOCUMENTATION PAGE

Form Approved OMB No. 0704-0188

1. REPORT DATE *(DD-MM-YYYY)*	2. REPORT TYPE	3. DATES COVERED *(From - To)*
	Journal Article	2002

4. TITLE AND SUBTITLE
Nonadiabatic effects in a self-consistent Hartree model for electrons under an ac electric field in multiple quantum wells

5a. CONTRACT NUMBER

5b. GRANT NUMBER

5c. PROGRAM ELEMENT NUMBER
62601F

6. AUTHOR(S)
Danhong Huang and D.A. Cardimona

5d. PROJECT NUMBER
4846

5e. TASK NUMBER
CR

5f. WORK UNIT NUMBER
C1

7. PERFORMING ORGANIZATION NAME(S) AND ADDRESS(ES)

Air Force Research Laboratory
Space Vehicles Directorate
3550 Aberdeen Ave. SE
Kirtland AFB, NM 87117-5776

8. PERFORMING ORGANIZATION REPORT NUMBER

9. SPONSORING / MONITORING AGENCY NAME(S) AND ADDRESS(ES)

10. SPONSOR/MONITOR'S ACRONYM(S)

11. SPONSOR/MONITOR'S REPORT NUMBER(S)

12. DISTRIBUTION / AVAILABILITY STATEMENT
Approved for Public Release; Distribution is Unlimited.

13. SUPPLEMENTARY NOTES
Published in Physical Review B 67, 245306 (2003)

14. ABSTRACT

By deriving a dynamical differential equation for the electron distribution function in the presence of a nonadiabatic sequential-tunneling current under an ac electric field through a multiple-quantum-well system, the self-consistent Hartree model is generalized for the calculation of electronic states with the inclusion of nonadiabatic effects (dependence on the time derivative of the applied ac electric field) in quantum wells. The influence of different doping profiles, temperatures, and amplitudes of an applied ac electric field on the electron distribution function and sequential tunneling are studied. This work provides a fully quantum-mechanical explanation to the previously proposed current-surge model to a leading-order approximation.

15. SUBJECT TERMS
Nonuniform fields, multiple quantum wells, nonadiabatic

16. SECURITY CLASSIFICATION OF:			17. LIMITATION OF ABSTRACT	18. NUMBER OF PAGES	19a. NAME OF RESPONSIBLE PERSON
a. REPORT	b. ABSTRACT	c. THIS PAGE			Mr. David Cardimona
Unclassified	Unclassified	Unclassified	Unlimited	11	19b. TELEPHONE NUMBER *(include area code)* (505) 846-5807

Nonadiabatic effects in a self-consistent Hartree model for electrons under an ac electric field in multiple quantum wells

Danhong Huang and D. A. Cardimona
Air Force Research Laboratory (AFRO/VSSS), 3550 Aberdeen Avenue SE, Building 426, Kirtland Air Force Base, New Mexico 87117
(Received 12 August 2002; revised manuscript received 26 December 2002; published 11 June 2003)

By deriving a dynamical differential equation for the electron distribution function in the presence of a nonadiabatic sequential-tunneling current under an ac electric field through a multiple-quantum-well system, the self-consistent Hartree model is generalized for the calculation of electronic states with the inclusion of nonadiabatic effects (dependence on the time derivative of the applied ac electric field) in quantum wells. The influences of different doping profiles, temperatures, and amplitudes of an applied ac electric field on the electron distribution function and sequential tunneling are studied. This work provides a fully quantum-mechanical explanation to the previously proposed current-surge model to a leading-order approximation.

DOI: 10.1103/PhysRevB.67.245306 PACS number(s): 73.40.Gk, 73.21.Fg, 73.40.Kp

I. INTRODUCTION

Recently, transient transport properties of semiconductor quantum wells,[1–3] superlattices[4,5] and quantum dots[6] have been a subject of interest. Various nonlinear properties having their origin in the Coulomb interaction have attracted a great deal of attention.[3,7–10] Self-sustained current oscillations and multistability have been predicted in tunneling currents through doped semiconductor superlattices and multiple quantum wells (MQW's).[7] They are attributed to the dynamics of domain walls separating the electric-field domains. In addition, oscillations in the sequential-tunneling current have been predicted in MQW's, even in the absence of electric-field domains due to nonadiabatic effects.[10] The nonadiabatic effects discussed in this paper are associated with the fact that a transient conduction current depends not only on an electric field but also on its time derivative due to quantum-well capacitive coupling. The quantum-well capacitance is of the order of picofarads. However, the resistance of the MQW sample with a thick barrier between the wells used in this study is of the order of teraohms due to the extremely small sequential-tunneling current. As a result, the nonadiabatic effect occurs on a time scale of seconds, which makes electron tunneling depend on the time derivative of the applied electric field in addition to the field itself for low ac frequencies of the order of a few hertz.[11,12]

In this paper, we consider the sequential-tunneling transport of electrons in an MQW system in the presence of an applied ac electric field. We assume that the lattice temperature is kept constant and the electrons are in thermal equilibrium with the lattice, so that the electron temperature is the same as that of the lattice. The sequential tunneling of electrons (of the order of nanoseconds) through a thick barrier between adjacent quantum wells in an MQW system is a very slow process as compared to the coherent tunneling of electrons (of the order of sub-picoseconds) through a thin barrier in a superlattice system. However, electrons during the sequential-tunneling process still "see" an instantaneous electric field because of $\tau_t \ll 2\pi/\Omega$ for low ac frequency Ω (of the order of a few hertz) with τ_t being the sequential-tunneling time (of the order of nanoseconds).

Adiabatic electrons in an MQW system with an applied ac electric field stay in the equilibrium states with a constant Fermi level, since $\tau_e \ll \tau_t$, with τ_e being the energy-relaxation time due to the very-long sequential-tunneling time within which an equilibrium state can be established by the much faster inelastic scattering of electrons inside the quantum well. However, the electron density can vary with time if the electrons in the quantum well stay in the nonadiabatic state.[10,13,14] For the nonadiabatic state, the nonadiabatic effects cause the Fermi level in the "equilibrium" state to shake with time under an ac electric field. As a result, a charge-density fluctuation in the quantum well will modify the Hartree potential in the surrounding barrier region, and thus greatly affect the sequential tunneling of electrons through the barrier. Simultaneously, the charge-density fluctuation also modifies the electronic states in the quantum well within the self-consistent Hartree model.[15]

For the quantum-well sample considered in this study, the second-subband edge is 83.4 meV above the first-subband edge (see Table I), while the Fermi level is only 14.2 meV above the first-subband edge (see Table II). As a result, the second subband is completely unpopulated at temperatures below 40 K. Therefore, we have neglected the tunneling contribution from the unpopulated second subband. The well-known negative differential conductance (NDC) phenomenon can be seen if the second subband in the quantum well is brought into consideration for electron tunneling. For the multisubband case, the NDC occurs at a field strength where the first-subband edge in the preceding well is aligned with the second-subband edge in the next tilted well (there is a very narrow spectral density for both quantum wells be-

TABLE I. Parameters of $GaAs/Al_xGa_{1-x}As$ MQW sample used for numerical calculations with well depth V_0, well width L_W, barrier thickness L_B, electron density n_{2D}, well (barrier) relative dielectric constant ϵ_W (ϵ_B), and well (barrier) electron effective mass m_W (m_B) with m_e being the free-electron mass.

V_0 (meV)	L_W (Å)	L_B (Å)	n_{2D} (10^{11} cm^{-2})	ϵ_W	ϵ_B	m_W (m_e)	m_B (m_e)
331	80	300	4.0	12.0	11.2	0.067	0.092

TABLE II. Calculated parameters of GaAs/$Al_xGa_{1-x}As$ MQW sample used for numerical calculations, including average electron effective mass m^* with m_e being the free-electron mass, zero-field ground-subband edge $E_1^{(0)}$, second-subband edge $E_2^{(0)}$, and chemical potential $\mu_0(n_{2D},T)$ measured from $E_1^{(0)}$.

m^* (m_e)	$E_1^{(0)}$ (meV)	$E_2^{(0)}$ (meV)	μ_0 (meV)
0.07	44.5	127.9	14.2

cause of the very thick barrier between them). On the other hand, the NDC phenomenon also occurs in quantum wells with a single subband. This is due to a lesser overlap between the quantum-well quasiparticle spectral functions (whose width depends not only on the interwell coupling but also on the disorder self-energy) as the applied electric field increases when the Fermi energy is not too far from the top of the barrier. For the sample with barrier thickness $L_B = 300$ Å considered in this paper, the required field strength for the multisubband NDC phenomenon is 27.8 kV/cm. However, the maximum field strength employed in this study is only 1 kV/cm. Consequently, we have only included the first subband and neglected the NDC effect in our model where the Fermi energy is well below the top of the barrier. Moreover, the field-domain effect in an MQW system is expected to be very small under low electric fields for coherent-tunneling cases or below 40 K for sequential-tunneling cases and is neglected in this paper since it becomes significant only for a large-tunneling current. The thick-barrier-layer sample used in this study is to limit the dark sequential-tunneling current to an extremely low amount, which ensures a very high detectivity for quantum-well infrared photodetectors operating at a low-temperature and/or a low-photon background.[16] When the sequential tunneling is low, the impurity or defect channels within the barrier would play a role.[17] However, this only modifies the resistance of the sample for sequential tunneling of electrons. The nonadiabatic effects discussed in this paper for electron tunneling remain the same. The usual self-consistent Hartree model is based on the known equilibrium (Fermi-Dirac) distribution function of electrons, which can be applied to find electron wave functions and energy levels simultaneously in quantum wells. The main result of this paper is the derivation of a dynamical differential equation for nonadiabatic electrons under an ac electric field in quantum wells which is then used to find the electron distribution function. This dynamical equation can be coupled to the self-consistent Hartree model to solve for electron wave functions, energy levels, and nonadiabatic distributions at the same time.

The paper is organized as follows. In Sec. II, we introduce a shifted Fermi-Dirac model[18] for local fluctuations of electron kinetic energy and charge density in the quantum well. Section III is used to establish a unified theory for both coherent and sequential tunneling of electrons in quantum-well and superlattice systems. The previous current-surge model is briefly reviewed in Sec. IV. Section V is devoted to the derivation of a differential equation based on the self-consistent Hartree model with the inclusion of nonadiabatic effects on the electron distribution function, and to the establishment of the connection between the current quantum theory and the previous current-surge model. Numerical results and discussions are given in Sec. VI for the changes of current, drift velocity, and density as a function of time. The electron distribution functions at different times for various temperatures, amplitudes of ac electric field, and doping profiles are also shown and compared. The paper is concluded in Sec. VII with some remarks.

II. SHIFTED FERMI-DIRAC MODEL

By using a shifted Fermi-Dirac model,[18] the nonequilibrium electron distribution function can be written as

$$f^{\mu_0}(\mathbf{k}) = f_0^{\mu_0}(E_{|\mathbf{k}+\Delta\mathbf{k}|} + \Delta E_k), \tag{1}$$

where $f_0^{\mu_0}(E_k)$ is the Fermi function and is given by

$$f_0^{\mu_0}(E_k) = \left\{1 + \exp\left[\frac{E_k - \mu_0(n_{2D},T)}{k_B T}\right]\right\}^{-1}. \tag{2}$$

Here, E_k is the electron kinetic energy and T is the temperature. $\mu_0(n_{2D},T)$ is the chemical potential of the equilibrium electron gas relative to the edge of the ground subband in the quantum well and is determined by the electron density n_{2D} at T. In Eq. (1), ΔE_k represents the local fluctuation of electron kinetic energy for electron state $|\mathbf{k}\rangle$. Using the acceleration theorem for the momentum drift $\Delta\mathbf{k}$ introduced in Eq. (1) under an applied electric field $\mathcal{E}_b(t)$, we obtain the following generalized Boltzmann's equation associated with the shifted Fermi-Dirac model in Eq. (1):

$$\frac{\partial f^{\mu_0}(\mathbf{k})}{\partial t} - \frac{e}{\hbar}\mathcal{E}_b(t)\nabla_k E_k \frac{\partial f^{\mu_0}(\mathbf{k})}{\partial E_k} + \frac{d\Delta E_k}{dt}\frac{\partial f^{\mu_0}(\mathbf{k})}{\partial E_k} = \frac{\partial f^{\mu_0}(\mathbf{k})}{\partial t}\Big|_{\text{coll}}, \tag{3}$$

where $\mathcal{E}_b(t) = \mathcal{E}_{dc} + \mathcal{E}_{ac}\sin(\Omega t)$ is the time-dependent electric field with frequency $\Omega = 2\pi/T_p$, time period T_p, dc amplitude $\mathcal{E}_{dc}$, and ac amplitude $\mathcal{E}_{ac}$. The term on the right-hand side of Eq. (3) represents collision contributions. In the limit of $\Omega\tau_e \ll 1$ with τ_e being the energy-relaxation time of electrons in the quantum well, we have $\langle d\Delta E_k/dt\rangle_t = 0$; but $\langle d\Delta\mathbf{k}/dt\rangle_t = e\mathcal{E}_b(t)/\hbar$, where $\langle\cdots\rangle_t$ defines a time average over multiple periods of T_p. In this case, only the momentum-drift phenomenon occurs. On the other hand, we find $\langle d\Delta\mathbf{k}/dt\rangle_t = 0$ in the limit of $\Omega\tau_p \gg 1$, with τ_p being the momentum-relaxation time of electrons in the quantum well. Under this condition, only the energy-drift phenomenon occurs with $\langle d\Delta E_k/dt\rangle_t = \sigma(\Omega)\mathcal{E}_{ac}^2/4$, where $\sigma(\Omega)$ is the ac conductivity of electrons in the quantum well.[19]

For the shifted Fermi-Dirac model in Eq. (1), there exists a local charge-density fluctuation for each electron state $|\mathbf{k}\rangle$, defined by

$$\frac{d}{dt}\delta\rho_{\mathbf{k}}(t)=\frac{d}{dt}\left\{\frac{e}{\mathcal{V}}[f^{\mu_0}(\mathbf{k})-f_0^{\mu_0}(E_k)]\right\}$$

$$=-\frac{e}{\mathcal{V}}\left\langle\frac{d\Delta E_k}{dt}\right\rangle_t\left[-\frac{\partial f_0^{\mu_0}(E_k)}{\partial E_k}\right], \quad (4)$$

where $\mathcal{V}$ is the volume of the sample. The local charge-density fluctuation is a result of the change of the electron distribution in energy space with respect to the equilibrium state even when n_{2D} is a constant.

III. COHERENT- AND SEQUENTIAL-TUNNELING MODELS

For an MQW system with thick-barrier layers, the adiabatic sequential-tunneling current density flowing in the z direction (growth direction and perpendicular to the quantum-well layers) is found to be[20]

$$J^{\mu_0}(t)=\frac{2e}{\mathcal{V}}\sum_{\mathbf{k}} v_k^z\mathcal{T}[E_k,\mathcal{E}_b][f^{\mu_0}(E_k)-f^{\mu_0}(E_k+e\mathcal{E}_bL_B)], \quad (5)$$

where L_B is the thickness of the barrier between two adjacent quantum wells, v_k^z is the group velocity of quasibound- or continuum-state electrons in the z direction, and $\mathcal{T}[E_k,\mathcal{E}_b]$ is the quantum-mechanical transmission of electrons through the biased barrier. If $\Omega\tau_t\gg 1$, with τ_t being the electron sequential-tunneling time, $\mathcal{T}[E_k,\mathcal{E}_b]$ has to be found by solving a time-dependent Schrödinger equation. Otherwise, $\mathcal{T}[E_k,\mathcal{E}_b]$ can be calculated from a static Schrödinger equation at each time t if $\Omega\tau_t\ll 1$. We will be only interested in the latter case with $\Omega\tau_t\ll 1$ hereafter.

In the limit of small barrier thickness and weak field, i.e., $e\mathcal{E}_bL_B\ll E_k$, Eq. (5) yields a coherent-tunneling current that takes the same form as that obtained using the regular Boltzmann's equation ($d\Delta E_k/dt=0$) under the relaxation-time approximation:

$$J^{\mu_0}(t)=\frac{2e^2}{\mathcal{V}}\mathcal{E}_b\sum_{\mathbf{k}}(v_k^z)^2\tau_p\left[-\frac{\partial f^{\mu_0}(E_k)}{\partial E_k}\right], \quad (6)$$

where we have set $\mathcal{T}[E_k,\mathcal{E}_b]=v_k^z\tau_p/L_B\ll 1$ for scattering-limited miniband-state electrons at very low electric field (with mean free path $v_k^z\tau_p$ smaller than L_B), and τ_p is the momentum-relaxation time of electrons. Consequently, the conductance that is proportional to $J^{\mu_0}(t)/\mathcal{E}_b$ becomes independent of $\mathcal{E}_b$ in this situation.

If we replace $f^{\mu_0}(E_k)$ to the leading-order approximation by the equilibrium value $f_0^{\mu_0}(E_k)$ for faster electron energy relaxation processes due to inelastic scattering of electrons as compared to the electron sequential tunneling, and replace the electron group velocity v_k^z by a drift velocity $v_d[\mathcal{E}_b]$ (a statistically averaged group velocity) of electrons in a bulk material, Eq. (5) reduces to Levine's sequential-tunneling model[20]

$$J^{\mu_0}[\mathcal{E}_b]=\frac{2e}{\mathcal{V}}v_d[\mathcal{E}_b]\sum_{\mathbf{k}}\mathcal{T}[E_k,\mathcal{E}_b][f_0^{\mu_0}(E_k)-f_0^{\mu_0}(E_k+e\mathcal{E}_bL_B)], \quad (7)$$

where $v_d[\mathcal{E}_b]=(e\tau_p/m^*)\mathcal{E}_b$, the momentum-relaxation time τ_p is given by

$$\tau_p=\frac{m^*v_s}{e\sqrt{\mathcal{E}_s^2+\mathcal{E}_b^2}}, \quad (8)$$

m^* is the effective mass of electrons, v_s is the electron saturation velocity, and $\mathcal{E}_s$ is the saturation electric field. In Eq. (7), $J^{\mu_0}[\mathcal{E}_b]/ev_d[\mathcal{E}_b]$ can be equivalently viewed as a three-dimensional tunneling-electron density that depends on $\mathcal{E}_b$, T, and n_{2D}. Obviously, the conductance that is proportional to $J^{\mu_0}[\mathcal{E}_b]/\mathcal{E}_b$ becomes dependent on $\mathcal{E}_b$ in this situation.

IV. CURRENT-SURGE MODEL

From now on, we limit ourselves to an electrical-quantum limit where only the ground subband of the narrow quantum well is occupied by electrons at low temperatures and low electron densities. The electron kinetic energy of the ground subband (measured from the edge) is given by $E_k=\hbar^2k^2/2m^*$. In the current-surge model,[10,13,14] we assume that ΔE_k is associated with the fluctuation of the chemical potential of electrons in the quantum well (independent of individual electron state), instead of the local fluctuation of electron kinetic energy for each electron state. By writing $\Delta E_k=-\Delta\mu=\mu_0(n_{2D},T)-\mu(t)$ for the global chemical-potential fluctuation, where $\mu(t)$ and $\mu_0(n_{2D},T)$ are, respectively, the transient chemical potential for electron density $n_e(t)$ and that for an equilibrium electron gas in quantum wells, we get

$$\frac{d\Delta E_k}{dt}=\frac{\partial\Delta E_k}{\partial t}-\frac{\partial\mu}{\partial n_e}\frac{dn_e}{dt}. \quad (9)$$

We further introduce a spatially averaged space-charge field $\mathcal{E}_{na}(t)$ which is defined by[10,13,14]

$$\Delta E_k=e\mathcal{E}_{na}(t)L_B, \quad (10)$$

where $\mathcal{E}_{na}(t)$ measures the reduction of the electron chemical potential in quantum wells. If we use Levine's sequential-tunneling model in Eq. (7), we find the change in the current density due to the existence of this space-charge field $\mathcal{E}_{na}(t)$,

$$\Delta J_{na}(t)=J^{\mu_0-eL_B\mathcal{E}_{na}}[\mathcal{E}_b+\mathcal{E}_{na}]-J^{\mu_0}[\mathcal{E}_b], \quad (11)$$

where $J^{\mu_0}[\mathcal{E}_b]$ has been given in Eq. (7). In Eq. (11), the first term can be viewed as an equivalent capture current flowing into the quantum well, while the second term can be regarded as a sequential-tunneling current flowing out of the quantum well.

For a quantum well, the electron density will be constant if the conduction currents flowing in and out of the well are equal. The variation of the charge density in the well is cre-

ated by an imbalance in conduction currents. The charge-current conservation law for density fluctuation $\delta\rho(t)$ requires

$$\mathcal{V}\frac{d}{dt}\delta\rho(t)\equiv\mathcal{V}\frac{d}{dt}\sum_{\mathrm{k}}\delta\rho_{\mathrm{k}}(t)=\mathcal{A}\Delta J_{\mathrm{na}}(t), \tag{12}$$

where $\mathcal{A}$ is the cross-sectional area of the MQW sample. The left-hand side of Eq. (12) represents the charge increase inside the well, while the right-hand side of the equation stands for the net increase in charges due to a nonadiabatic change in the current flowing into the quantum well. Combining Eqs. (4), (9), (10), and (12), we finally arrive at the following equation derived previously as the current-surge model:[10]

$$L_{\mathrm{B}}C_{\mathrm{QW}}\frac{d}{dt}\mathcal{E}_{\mathrm{na}}(t)=L_{\mathrm{B}}C_{\mathrm{QW}}\frac{d}{dt}\mathcal{E}_{\mathrm{b}}(t)-\Delta J_{\mathrm{na}}(t), \tag{13}$$

where the quantum-well capacitance per unit area is $C_{\mathrm{QW}}=(m^*e^2/\pi\hbar^2)f_0^{\mu_0}(0)$. Here, we have employed in Eq. (13) the fact that $(\partial\mu/\partial n_{\mathrm{e}})(dn_{\mathrm{e}}/dt)=eL_{\mathrm{B}}[d\mathcal{E}_{\mathrm{b}}(t)/dt]$ for the capacitance coupling of the quantum well to an external ac electric field.[10,13,14] The fast inelastic scattering in quantum wells ensures that electrons are in an "equilibrium" state. However, Eq. (13) causes a shaking Fermi level for the equilibrium state on a macroscopic time scale.

V. NONADIABATIC EFFECTS IN A SELF-CONSISTENT HARTREE MODEL

As mentioned in the Introduction, electrons in quantum wells see only the instantaneous ac electric field during their sequential-tunneling process if $\Omega\tau_{\mathrm{t}}\ll 1$. In this case, the ground-state electron wave function $\phi_1(z,t)$ inside the quantum well within the self-consistent Hartree model is determined by[21]

$$\left[-\frac{\hbar^2}{2}\frac{d}{dz}\left(\frac{1}{m^*(z)}\frac{d}{dz}\right)-e\mathcal{E}_{\mathrm{b}}(t)z+U_{\mathrm{QW}}(z)+\mathcal{V}_{\mathrm{H}}(z,t)\right]\phi_1(z,t)=E_1(t)\,\phi_1(z,t), \tag{14}$$

where $E_1(t)$ is the time-dependent ground-subband edge, the electron effective mass $m^*(z)$ takes m_{W} in the well and m_{B} in the barrier, and $U_{\mathrm{QW}}(z)$ is zero inside the well but V_0 outside the well. For the adiabatic state, we have $\mu(t)=\mu_0(n_{2\mathrm{D}},T)$, otherwise $\delta\rho(t)\neq 0$ for the cases with nonadiabatic effects. The Hartree potential $\mathcal{V}_{\mathrm{H}}(z,t)$ in Eq. (14) can be found from the Poisson equation

$$\frac{d}{dz}\left[\epsilon_{\mathrm{r}}(z)\frac{d}{dz}\mathcal{V}_{\mathrm{H}}(z,t)\right]=\frac{e^2}{\epsilon_0}[N_{\mathrm{D}}(z)-n_{\mathrm{e}}(z,t)], \tag{15}$$

where donors are assumed completely ionized, and the relative dielectric constant $\epsilon_{\mathrm{r}}(z)$ takes ϵ_{W} in the well and ϵ_{B} in the barrier. $N_{\mathrm{D}}(z)$ in Eq. (15) is the static profile of donor doping for the single quantum well, $n_{\mathrm{e}}(z,t)=|\phi_1(z,t)|^2n_{\mathrm{e}}(t)$ is the density function, and

$$n_{\mathrm{e}}(t)=n_{2\mathrm{D}}+\frac{\delta\rho(t)L_{\mathrm{W}}}{e}=n_{2\mathrm{D}}+\rho_{2\mathrm{D}}\int_0^{+\infty}dE\,\delta f(E,t), \tag{16}$$

where $\rho_{2\mathrm{D}}=(m_{\mathrm{W}}/\pi\hbar^2)$ is the density of states for two-dimensional electrons in the quantum well and $\delta f(E,t)$ represents the local fluctuation of the electron distribution function in energy space. Here, the number of electrons in the quantum well is not a constant due to the nonadiabatic current flowing. Moreover, we find from Eqs. (4), (9), and (16) that

$$L_{\mathrm{W}}\frac{d}{dt}\delta\rho(t)=e\rho_{2\mathrm{D}}\int_0^{+\infty}dE\frac{\partial}{\partial t}\delta f(E,t)+e^2L_{\mathrm{B}}\rho_{2\mathrm{D}}\frac{d}{dt}\mathcal{E}_{\mathrm{b}}(t)\int_0^{+\infty}dE\left[-\frac{\partial f_0^{\mu_0}(E)}{\partial E}\right]. \tag{17}$$

Applying Eq. (12) and using Eqs. (11) and (17), we find the following integral equation for $\delta f(E,t)$ by using Levine's model in Eq. (7)

$$\begin{aligned}
&e\rho_{2\mathrm{D}}\int_0^{+\infty}dE\frac{\partial}{\partial t}\delta f(E,t)+e^2L_{\mathrm{B}}\rho_{2\mathrm{D}}\frac{d\mathcal{E}_{\mathrm{b}}(t)}{dt}\\
&\times\int_0^{+\infty}dE\left[-\frac{\partial f_0^{\mu_0}(E)}{\partial E}\right]-\left(\frac{e\rho_{2\mathrm{D}}}{L_{\mathrm{W}}}\right)\{v_{\mathrm{d}}[\mathcal{E}_{\mathrm{b}}]+\delta v_{\mathrm{d}}[\delta f]\}\\
&\times\int_0^{+\infty}dE\mathcal{T}[E+E_1,\mathcal{E}_{\mathrm{b}};\mathcal{V}_{\mathrm{H}}][f_0^{\mu_0}(E)+\delta f(E,t)\\
&-f_0^{\mu_0}(E+e\mathcal{E}_{\mathrm{b}}L_{\mathrm{B}})-\delta f(E+e\mathcal{E}_{\mathrm{b}}L_{\mathrm{B}},t)]\\
&+\left(\frac{e\rho_{2\mathrm{D}}}{L_{\mathrm{W}}}\right)v_{\mathrm{d}}[\mathcal{E}_{\mathrm{b}}]\int_0^{+\infty}dE\mathcal{T}[E+E_1^{(0)},\mathcal{E}_{\mathrm{b}};\mathcal{V}_{\mathrm{H}}^{(0)}][f_0^{\mu_0}(E)\\
&-f_0^{\mu_0}(E+e\mathcal{E}_{\mathrm{b}}L_{\mathrm{B}})]=0.
\end{aligned} \tag{18}$$

In Eq. (18), $\mathcal{V}_{\mathrm{H}}(z,t)$ and $E_1(t)$ are written simply as $\mathcal{V}_{\mathrm{H}}$ and E_1. The adiabatic quantities $\mathcal{V}_{\mathrm{H}}^{(0)}(z,t)$ and $E_1^{(0)}(t)$ can be obtained by simply setting $\delta\rho(t)=0$ in Eq. (15) and $\mathcal{V}_{\mathrm{H}}(z,t)=\mathcal{V}_{\mathrm{H}}^{(0)}(z,t)$ in Eq. (14). Moreover, the fluctuation of the drift velocity $\delta v_{\mathrm{d}}[\delta f]$ introduced in Eq. (18) is calculated to be

$$\delta v_{\mathrm{d}}[\delta f]=-\left(\frac{\rho_{2\mathrm{D}}}{n_{2\mathrm{D}}}\right)\int_0^{+\infty}dE\,\delta f(E,t)\sqrt{\frac{2E}{m_{\mathrm{W}}}}. \tag{19}$$

Finally, Eq. (18) leads us to the dynamical differential equation for $\delta f(E,t)$,

$$\frac{\partial}{\partial t}\delta f(E,t)-eL_B\frac{d\mathcal{E}_b(t)}{dt}\frac{\partial f_0^{\mu_0}(E)}{\partial E}-\frac{1}{L_W}\times\{v_d[\mathcal{E}_b]+\delta v_d[\delta f]\}\mathcal{T}[E+E_1,\mathcal{E}_b;\mathcal{V}_H][f_0^{\mu_0}(E)+\delta f(E,t)-f_0^{\mu_0}(E+e\mathcal{E}_bL_B)-\delta f(E+e\mathcal{E}_bL_B,t)]+\frac{1}{L_W}v_d[\mathcal{E}_b]\mathcal{T}[E+E_1^{(0)},\mathcal{E}_b;\mathcal{V}_H^{(0)}][f_0^{\mu_0}(E)-f_0^{\mu_0}(E+e\mathcal{E}_bL_B)]=0, \quad (20)$$

where the initial condition is chosen to be $\delta f(E,t)=0$ at $t=0$ if the ac electric field is applied to the system after $t=0$. $\delta f(E,t)$ has a lower bound that is set by the condition $\delta f(E,t)+f_0^{\mu_0}(E)=0$.

For small $\Delta\mu$, the first term in Eq. (20) can be approximated to the leading order by

$$\frac{\partial}{\partial t}\delta f(E,t)\approx\frac{\partial\Delta\mu}{\partial t}\left[-\frac{\partial f_0^{\mu_0}(E)}{\partial E}\right]. \quad (21)$$

Similarly, a part of the third term in Eq. (20) can be approximated as

$$\mathcal{T}[E+E_1,\mathcal{E}_b;\mathcal{V}_H][f_0^{\mu_0}(E)+\delta f(E,t)-f_0^{\mu_0}(E+e\mathcal{E}_bL_B)-\delta f(E+e\mathcal{E}_bL_B,t)]\approx\mathcal{T}[E+E_1^{(0)},\mathcal{E}_b;\mathcal{V}_H^{(0)}+(\delta\mathcal{V}_H^{(0)}/\delta n_{2D})\rho_{2D}\Delta\mu]\times[f_0^{\mu_0+\Delta\mu}(E)-f_0^{\mu_0+\Delta\mu}(E+e\mathcal{E}_bL_B)], \quad (22)$$

where $(\delta\mathcal{V}_H^{(0)}/\delta n_{2D})=(e^2/2\epsilon_0\epsilon_W q_{TF})$ and $q_{TF}=(e^2/2\epsilon_0\epsilon_W)\rho_{2D}$ in the Thomas-Fermi model.[21] By recalling $\Delta\mu=-e\mathcal{E}_{na}(t)L_B$, Eq. (20) results in the current-surge model in Eq. (13), where

$$C_{QW}=e^2\rho_{2D}\int_0^{+\infty}dE\left[-\frac{\partial f_0^{\mu_0}(E)}{\partial E}\right],$$

$$J^{\mu_0}[\mathcal{E}_b]=\left(\frac{e\rho_{2D}}{L_W}\right)v_d[\mathcal{E}_b]\int_0^{+\infty}dE\mathcal{T}[E+E_1^{(0)},\mathcal{E}_b;\mathcal{V}_H^{(0)}]\times[f_0^{\mu_0}(E)-f_0^{\mu_0}(E+e\mathcal{E}_bL_B)],$$

$\mathcal{T}[E+E_1^{(0)},\mathcal{E}_b;\mathcal{V}_H^{(0)}-e\mathcal{E}_{na}L_B]\approx\mathcal{T}[E+E_1^{(0)},\mathcal{E}_b+\mathcal{E}_{na};\mathcal{V}_H^{(0)}]$, and $v_d[\mathcal{E}_b]+\delta v_d[\delta f]\approx v_d[\mathcal{E}_b+\mathcal{E}_{na}]$ if we set $\tau_p\approx L_B/(v_F/2)$ with v_F being the electron group velocity at the Fermi level. The space-charge field $\mathcal{E}_{na}(t)$ introduced by $\Delta\mu=-e\mathcal{E}_{na}(t)L_B$ can be calculated from

$$\mathcal{E}_{na}(t)=-\left(\frac{1}{eL_B}\right)\int_0^{+\infty}dE\,\delta f(E,t), \quad (23)$$

which becomes positive if $\delta\rho(t)<0$.

The quantum-mechanical transmission coefficient $\mathcal{T}[E+E_1,\mathcal{E}_b;\mathcal{V}_H]$ used to evaluate the tunneling current in Eq. (7) can be found from the following backward iteration[8] at each time t

$$\phi_{j-1}(t)=\left\{2+\frac{1}{E_d}[U_j^B-e\mathcal{E}_b(t)(j-1)\Delta+V_j^H(t)-E-E_1(t)]\right\}\phi_j(t)-\phi_{j+1}(t) \quad (24)$$

for $1\leq j\leq N_B$, where $\phi_j(t)=\phi_1(z_j,t)$, $V_j^H(t)=V_H(z_j,t)$, $E_d=\hbar^2/2m_B\Delta^2$, $\Delta=L_B/N_B$ and N_B is the number of slabs (thickness Δ) within the barrier layer. Here, $U_j^B=0$ for $j=0$ and $j=N_B+1$. Otherwise, $U_j^B=V_0$. The ending boundary condition of Eq. (24) produces

$$\begin{bmatrix}\phi_{N_B+1}(t)\\ \phi_{N_B}(t)\end{bmatrix}=\begin{bmatrix}\exp(iN_B\bar{k}')\\ \{1-i\bar{k}'-(1/2E_d)[E+E_1(t)-U_{N_B+1}^B+e\mathcal{E}_b(t)N_B\Delta-V_{N_B+1}^H(t)]\}\phi_{N_B+1}(t)\end{bmatrix}, \quad (25)$$

where $\bar{k}'=(\Delta/\hbar)\sqrt{2m_B(E+e\mathcal{E}_b(t)L_B)}$. From the solution of Eq. (24) we find the quantum-mechanical transmission of electrons from

$$\mathcal{T}[E+E_1,\mathcal{E}_b;\mathcal{V}_H]=\frac{1}{|S|^2}\sqrt{\frac{E+e\mathcal{E}_b(t)L_B}{E}}, \quad (26)$$

where $|S|^2=[|a|^2+|b|^2+2\mathrm{Re}(ab^*)]/4$. The solution of Eq. (24) ensures that the transmission coefficient in Eq. (26) depends on the barrier thickness and height in an exponential way. Here, the two complex numbers a and b are defined by the starting boundary condition of Eq. (24)

$$\begin{bmatrix}a\\ b\end{bmatrix}=\begin{bmatrix}\phi_1(t)\\ -(i/2\bar{k})(\phi_2(t)-\phi_0(t))\end{bmatrix}, \quad (27)$$

with $\bar{k}=(\Delta/\hbar)\sqrt{2m_BE}$.

VI. NUMERICAL RESULTS AND DISCUSSION

We choose a GaAs/Al_xGa_{1-x}As MQW sample for numerical calculations. Some sample parameters can be found in Tables I and II. Other parameters include $\mathcal{E}_{dc}=0.05$ kV/cm, $v_s=2\times10^6$ cm/sec, $\mathcal{E}_s=2$ kV/cm, and $T_p=4$ sec. Different doping profiles have been considered, in-

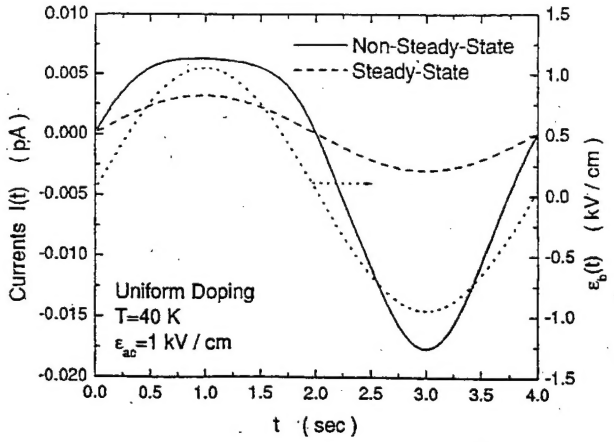

FIG. 1. Calculated time dependence of electron sequential-tunneling currents $I(t)=\mathcal{A}[J^{\mu_0}[\mathcal{E}_b]+\Delta J_{na}(t)]$ (left scale) for nonadiabatic [$\Delta J_{na}(t)\neq 0$, solid curve] and adiabatic [$\Delta J_{na}(t)=0$, dashed curve], and an applied ac electric field $\mathcal{E}_b(t)$ (right scale) for $T=40$ K and $\mathcal{E}_{ac}=1$ kV/cm with uniform doping inside GaAs quantum wells.

cluding uniform well doping, center δ doping, and edge δ doping. The temperature T and the amplitude of the ac electric field, $\mathcal{E}_{ac}$, will be given in the figure captions.

Figure 1 presents the calculated nonadiabatic electron sequential-tunneling current $I_{na}(t)=[J^{\mu_0}[\mathcal{E}_b]+\Delta J_{na}(t)]\mathcal{A}$ (solid curve) and the adiabatic sequential-tunneling current $I_a(t)=J^{\mu_0}[\mathcal{E}_b]\mathcal{A}$ (dashed curve) as a function of time t (left scale) for the MQW sample at $T=40$ K, $\mathcal{E}_{ac}=1$ kV/cm, and with uniform doping inside the GaAs quantum wells. For comparison, the applied ac electric field $\mathcal{E}_b(t)$ (right scale) is also plotted in the same figure. When $\mathcal{E}_b(t)$ approaches its maximum (i.e., $t=1$ sec), we find a small enhancement in $I_{na}(t)$ with respect to $I_a(t)$ and the saturation of $I_{na}(t)$ due to the large reduction in electron density inside the quantum wells. On the other hand, we find a large enhancement in $I_{na}(t)$ due to the large increase of electron density inside the quantum wells when $\mathcal{E}_b(t)$ approaches its minimum (i.e., $t=3$ sec). These features are a result of the induced space-charge field $\mathcal{E}_{na}(t)$.

The reduction of electron population around $E=\mu_0(n_{2D},T)$ can be described by the space-charge field $\mathcal{E}_{na}(t)$ defined in Eq. (23). We display $\mathcal{E}_{na}(t)$ (solid curve, left scale) in Fig. 2(a), along with $\mathcal{E}_b(t)$ (dashed curve, right scale) as functions of t for uniform doping. From the figure we see that $\mathcal{E}_{na}(t)$ and $\mathcal{E}_b(t)$ are nearly in phase with each other, except for a slight phase shift. This is a direct result of oscillations in the change of the charge density $\delta\rho(t)$ in the quantum well, as shown in Fig. 2(b), where both $\delta\rho(t)$ (solid curve, left scale) and $\delta v_d[\delta f]$ (dashed curve, right scale) are plotted as functions of t. Since $\mathcal{E}_{na}(t)$ describes the reduction of charge density in the quantum well, we expect $\delta\rho(t)$ to be nearly out of phase with $\mathcal{E}_{na}(t)$ or $\mathcal{E}_b(t)$, as can be seen from Figs. 2(a) and 2(b). The situations with $\delta\rho(t)<0$ and $\delta\rho(t)>0$ indicate electrons moving out of and into the quantum well, respectively. Moreover, $\delta v_d[\delta f]$ will be in phase with $\mathcal{E}_{na}(t)$ since it is proportional to $-\delta f(E,t)$ that itself is proportional to $\mathcal{E}_{na}(t)$.

Figure 3 displays the calculated adiabatic Hartree potential [in panel (a)] and the change of Hartree potential [in panel (b)] in the nonadiabatic state from the Poisson equation (15) as functions of position z for different doping profiles at $t/T_p=0.25$. Here, $T=40$ K, $\mathcal{E}_{ac}=1$ kV/cm, and the quantum well sits in the range of 300 Å$\leq z\leq$380 Å. From Fig. 3(a) we find that the absolute value of the adiabatic Hartree potential becomes smallest for the uniform-doping case. The center δ doping in the quantum well causes the conduction band edge to bend down at the well center, while the edge δ doping makes the conduction band edge bend up there, as shown in Fig. 3(a). With the total potential seen by the electrons being the sum of the adiabatic Hartree potential $V_H^{(0)}(z,t)$ plus the change $\Delta V_H(z,t)$ plus the quantum-well potential $U_{QW}(z)$, the out-of-phase nature of Figs. 3(a) and 3(b) will result in the band bending seen in Fig. 3(a) being substantially suppressed by the nonadiabatic effects in Fig. 3(b). However, the nonadiabatic effects with edge δ doping produces two positive spikes [solid curve in Fig. 3(b)] at the

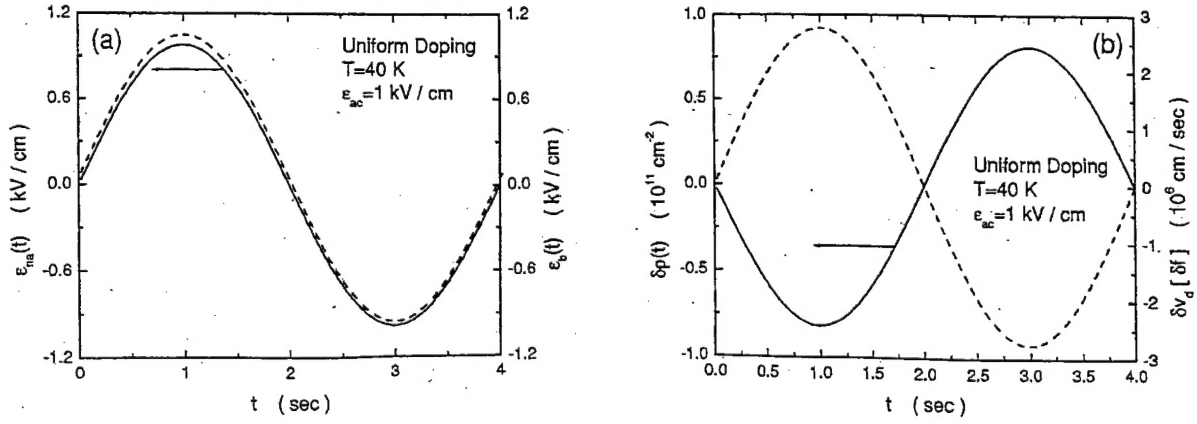

FIG. 2. Time dependence of a calculated space-charge field $\mathcal{E}_{na}(t)$ (solid curve, left scale) and an applied ac electric field $\mathcal{E}_b(t)$ (dashed curve, right scale) in panel (a), as well as time dependence of calculated charge-density fluctuation $\delta\rho(t)$ (solid curve, left scale) and change of drift velocity $\delta v_d[\delta f]$ (dashed curve, right scale) in panel (b) for $T=40$ K and $\mathcal{E}_{ac}=1$ kV/cm with uniform doping inside quantum wells.

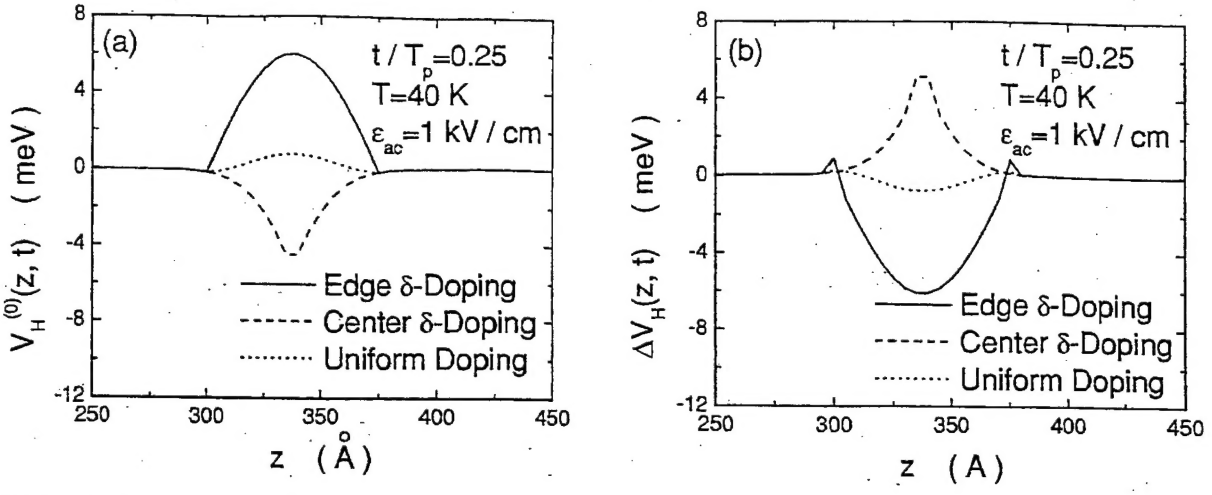

FIG. 3. Calculated position dependence of adiabatic Hartree potentials $V_H^{(0)}(z,t)$ in panel (a) and change of nonadiabatic Hartree potentials $\Delta V_H(z,t)$ in panel (b) at $t/T_p=0.25$, with $T=40$ K and $\mathcal{E}_{ac}=1$ kV/cm for edge δ doping (solid curves), center δ doping (dashed curves), and uniform doping (dotted curves) in the quantum well.

edges of the quantum well and thus will reduce the electron sequential-tunneling current.

Figure 4 indicates the effects of an ac electric-field strength $\mathcal{E}_{ac}$ [in panel (a)] and temperature T [in panel (b)] on the charge-density fluctuations $\delta\rho(t)$ as a function of t in a uniformly doped quantum well. In Fig. 4(a) we find that fluctuations $\delta\rho(t)$ increase with $\mathcal{E}_{ac}$ at $T=40$ K, with the negative peak (electrons removed from the quantum well) being saturated at $\mathcal{E}_{ac}=5$ kV/cm. In Fig. 4(b), as T increases $\delta\rho(t)$ is enhanced when it is negative (electrons removed from the quantum well), but reduced when it is positive (electrons added to the well) at $\mathcal{E}_{ac}=1$ kV/cm.

Figure 4 only shows us the global fluctuation of the charge density in the quantum well. In order to gain further insight into the local change in the electron distribution function, we display $\delta f(E,t)$ in Fig. 5 at $t/T_p=0.25$ with uniform doping for different values of $\mathcal{E}_{ac}$ [in panel (a)] and T [in panel (b)]. From Fig. 5(b) it is clear that $\delta f(E,t)$ always shows a negative minimum at $\mu_0(n_{2D},T)$, since it is proportional to $\partial f_0^{\mu_0}(E)/\partial E$. Because the Fermi surface broadens with increasing T, we find from Fig. 5(b) that the negative minimum is partially suppressed and broadened (solid curve) when $T=40$ K as compared to that (dashed curve) at $T=20$ K. From Fig. 5(a) we find that the negative minimum is enhanced when $\mathcal{E}_{ac}$ is increased. The cusp (dashed curve) in Fig. 5(a) is a result of zero occupation of electrons in a specific state with kinetic energy E in the ground subband.

Figures 6(a) and 6(b) present nonadiabatic effects on the Hartree potentials in the uniformly doped quantum well at $T=40$ K and $\mathcal{E}_{ac}=1$ kV/cm. From Fig. 6(a) we find that the positive peak in the adiabatic Hartree potential $V_H^{(0)}(z,t)$ (dashed curve) at the center of the quantum well is greatly suppressed by the nonadiabatic effects (solid curve) at $t/T_p=0.25$, leaving two positive spikes at the edges of the quan-

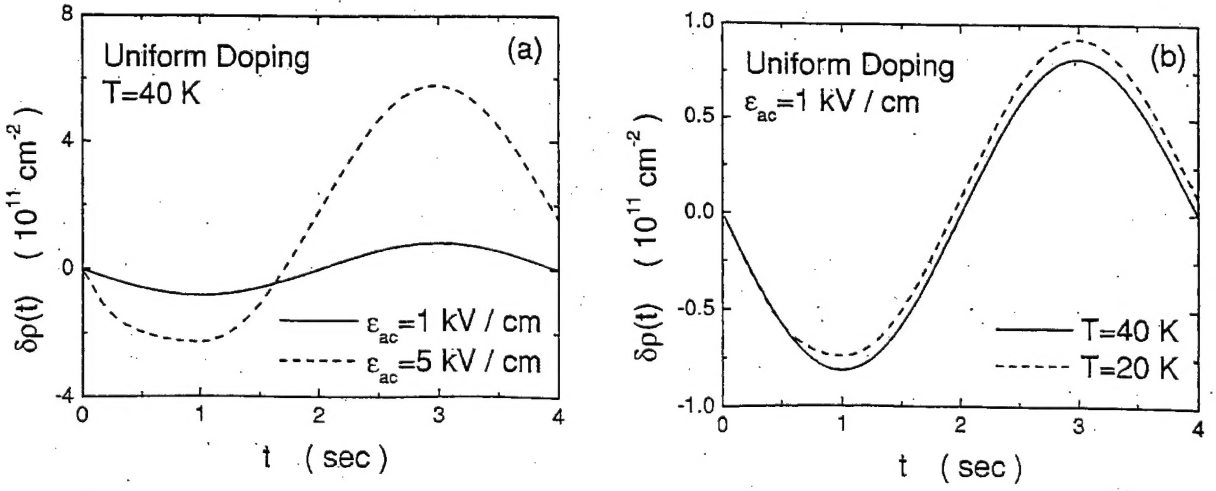

FIG. 4. Time dependence of calculated charge-density fluctuations $\delta\rho(t)$ in the uniformly doped quantum well . In panel (a), we set $T=40$ K with $\mathcal{E}_{ac}=1$ kV/cm (solid curve) and $\mathcal{E}_{ac}=5$ kV/cm (dashed curve). In panel (b), we set $\mathcal{E}_{ac}=1$ kV/cm with $T=40$ K (solid curve) and $T=20$ K (dashed curve).

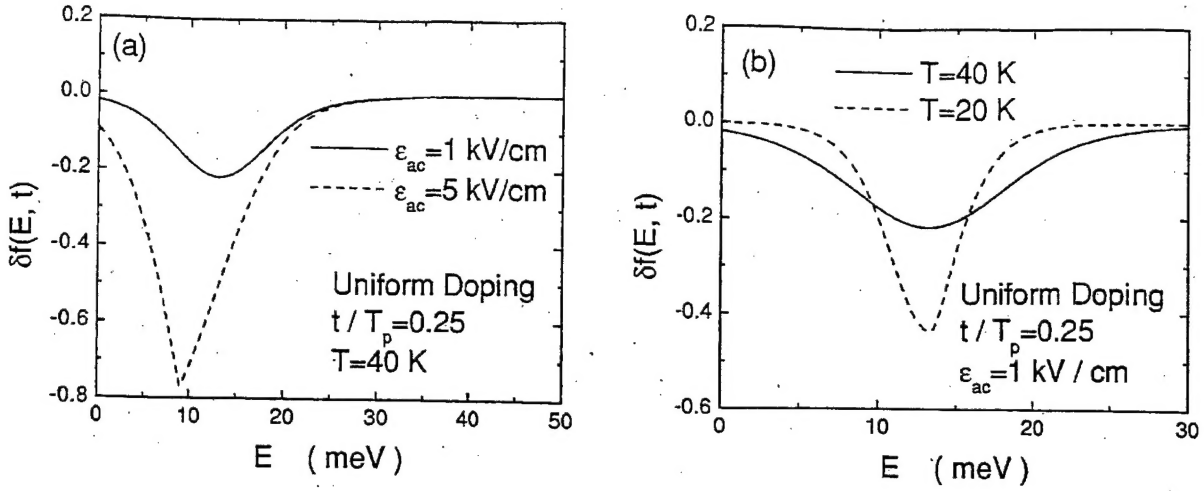

FIG. 5. Calculated change of nonadiabatic distribution functions $\delta f(E,t)$ at $t/T_p=0.25$ for electrons in the uniformly doped quantum well. In panel (a), we set $T=40$ K with $\mathcal{E}_{ac}=1$ kV/cm K (solid curve) and $\mathcal{E}_{ac}=5$ kV/cm (dashed curve). In panel (b), we set $\mathcal{E}_{ac}=1$ kV/cm with $T=40$ K (solid curve) and $T=20$ K (dashed curve).

tum well. Figure 6(b) shows the comparison between Hartree potentials when the electrons in the quantum well are either removed ($t/T_p=0.25$, solid curve) or added ($t/T_p=0.75$, dashed curve). We find from Fig. 6(b) that the two positive spikes at the edges of the quantum well are suppressed, but two negative spikes are generated when electrons are added to the well.

Finally, we display in Fig. 7 $f(E,t)$ at $t/T_p=0.25$ (dotted curve) and 0.75 (dashed curve), as well as the equilibrium distribution $f_0^{\mu_0}(E)$ (solid curve) in panel (a) and $\log_{10}|I_{na}(t)|$ as a function of $\mathcal{E}_b(t)$ in panel (b). From Fig. 7(a) we see $f(E,t)$ resembles the equilibrium distribution $f_0^{\mu_0}(E)$ with a shaking Fermi level with time (shaking up at $t/T_p=0.75$ and shaking down at $t/T_p=0.25$). Compared with the adiabatic electron sequential-tunneling current [thin solid curve with $\Delta J_{na}(t)=0$] in Fig. 7(b), the symmetry of $\log_{10}|I_{na}(t)|$ with respect to the positive (electrons being removed) and negative (electrons being added) extreme values of $\mathcal{E}_b(t)$ is broken in the case with nonadiabatic effects (thick solid curve). A small offset[10,13,14] of $\log_{10}|I_{na}(t)|$ with respect to $\mathcal{E}_b(t)=0$ can be seen by comparing thick and thin solid curves.

VII. CONCLUSIONS AND REMARKS

In conclusion, we have derived a dynamical differential equation for the nonadiabatic electron distribution function with sequential-tunneling current flowing through an MQW system. Using this equation, we generalized the self-consistent Hartree model for the calculation of the electronic states with the inclusion of nonadiabatic effects in a quantum well. We have also studied the effects of different doping profiles, temperatures, and amplitudes of applied ac electric field on the nonadiabatic electron sequential tunneling. Fi-

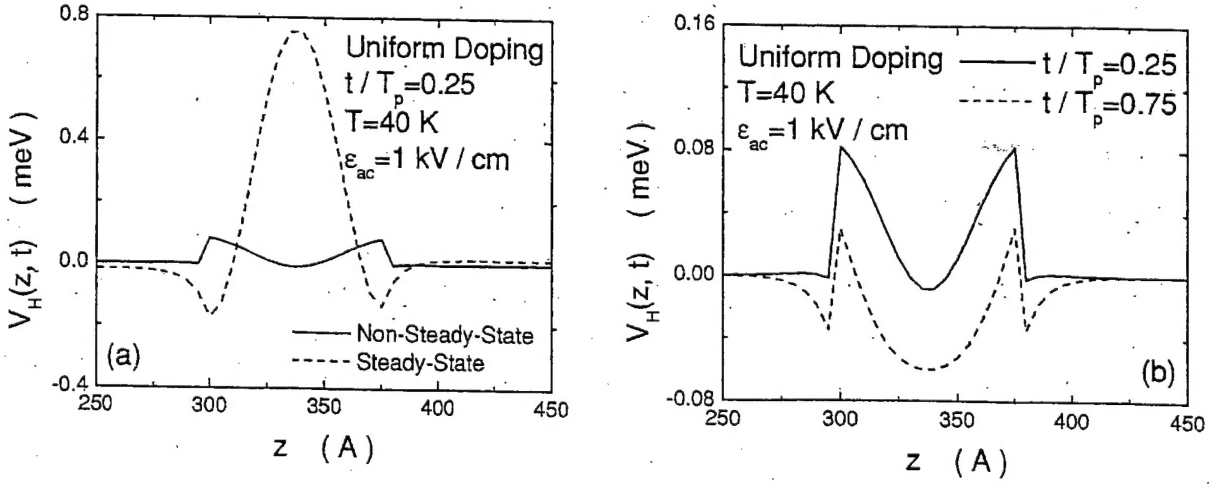

FIG. 6. Calculated position dependence of Hartree potentials for nonadiabatic (solid curve) and adiabatic (dashed curve) in panel (a) at $T=40$ K and $\mathcal{E}_{ac}=1$ kV/cm with uniform doping inside the quantum well, and nonadiabatic Hartree potentials $V_H(z,t)$ in panel (b) for $t/T_p=0.25$ (solid curve) and $t/T_p=0.75$ (dashed curve).

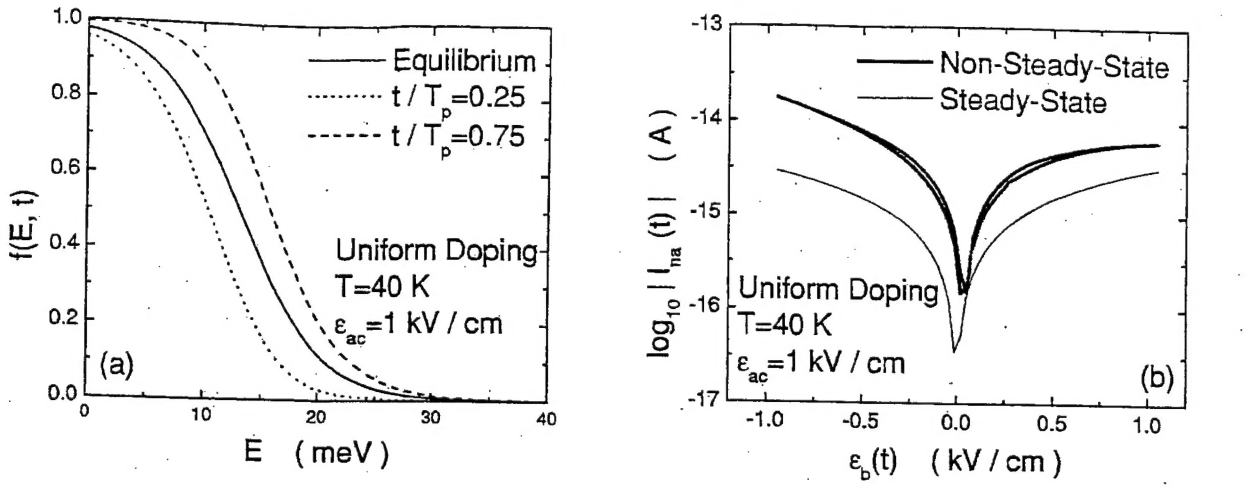

FIG. 7. Calculated nonadiabatic electron distribution functions $f(E,t)$ in panel (a) and logarithm of absolute value of nonadiabatic sequential-tunneling current $I_{na}(t)=\mathcal{A}[J^{\mu_0}[\mathcal{E}_b]+\Delta J_{na}(t)]$ as a function of an applied ac electric field $\mathcal{E}_b(t)$ in panel (b) for $T=40$ K and $\mathcal{E}_{ac}=1$ kV/cm. In panel (a), we plot $f(E,t)$ at $t/T_p=0.25$ (dotted curve) and $t/T_p=0.75$ (dashed curve). The equilibrium electron distribution function $f_0^{\mu_0}(E)$ (solid curve) is also shown for the comparison. In panel (b), the currents calculated from adiabatic (thin curve) and nonadiabatic (thick curve) electron sequential tunneling are compared with each other.

nally, we have connected the present quantum-statistical theory to the previously proposed current-surge model with a leading-order approximation.

In this paper, only the self-consistent Hartree model is employed. The exchange interaction between electrons and the field-domain effect are expected to be very small[22] at $T=40$ K and $\mathcal{E}_{ac}=1$ kV/cm and have been neglected.

The time scale for observing the nonadiabatic effects requires

$$\tau_e \ll \tau_t \ll t < R_t C_{QW} \mathcal{A}, \quad 2\pi/\Omega,$$

where $R_t=(L_B/\mathcal{A})[\partial J^{\mu_0}[\mathcal{E}_b]/\partial \mathcal{E}_b]^{-1}$ is the differential tunneling resistance, depending on $\mathcal{E}_b$ and T. Here, $\Omega\tau_e \ll 1$ excludes the energy-drift effect, leaving only the momentum-drift effect in the system. Further, $\Omega\tau_t \ll 1$ ensures that the electrons see only an instantaneous ac electric field during the sequential-tunneling process. Finally, $t<R_tC_{QW}\mathcal{A}$ ensures the observation of the nonadiabatic effects inside the quantum well. Assuming $\tau_e=1$ ps corresponds to a homogeneous energy-level broadening of 1 meV, leading to $\Omega \ll 10^{12}$ Hz from $\Omega\tau_e \ll 1$. Therefore, only a momentum drift exists for low ac frequency $\Omega \sim 1$ Hz. The tunneling time τ_t can be estimated from $\tau_t \sim e/[J^{\mu_0}[\mathcal{E}_b]\mathcal{A}]$. For a superlattice, we take $J^{\mu_0}[\mathcal{E}_b]\mathcal{A}=1$ μA, leading to $\tau_t=0.1$ ps and $\Omega \ll 10^{13}$ Hz from $\Omega\tau_t \ll 1$. For an MQW system, we take $J^{\mu_0}[\mathcal{E}_b]\mathcal{A}=10$ pA, leading to $\tau_t=10$ ns and $\Omega \ll 10^8$ Hz. This justifies the calculation of the quantum-mechanical transmission of electrons through a biased barrier using the time-independent Schrödinger equation in an MQW system with $\Omega \sim 1$ Hz. Difficulties in observing the nonadiabatic effects may come from the small quantum-well capacitance $C_{QW}\mathcal{A} \sim 10$ pF in the requirement $t<R_tC_{QW}\mathcal{A}$. For a superlattice, we take $R_t=10^4$ ohm, and then $t<10^{-7}$ sec is required (impossible to observe with $\Omega \sim 1$ Hz). For an MQW system, on the other hand, we take $R_t=10^{11}$ ohm, which implies $t<1$ sec (very easy to observe with $\Omega \sim 1$ Hz).

[1] M. Ershov, V. Ryzhii, and C. Hamaguchi, Appl. Phys. Lett. **67**, 3147 (1995).
[2] L. Thibaudeau, P. Bois, and J.Y. Duboz, J. Appl. Phys. **79**, 446 (1996).
[3] R. Aguado, G. Platero, M. Moscoso, and L. Bonilla, Phys. Rev. B **55**, R16 053 (1997).
[4] D.H. Dunlap and V.M. Kenkre, Phys. Rev. B **37**, 6622 (1988).
[5] X.-G. Zhao, G.A. Georgakis, and Q. Niu, Phys. Rev. B **54**, R5235 (1996).
[6] Q.-F. Sun and T.-H. Lin, Phys. Rev. B **56**, 3591 (1997).
[7] D. Sánchez, M. Moscoso, L. Bonilla, G. Platero, and R. Aguado, Phys. Rev. B **60**, 4489 (1999).
[8] D.H. Huang, D.A. Cardimona, and A. Singh, Phys. Lett. A **243**, 335 (1998).
[9] R. Aguado and G. Platero, Phys. Rev. Lett. **81**, 4971 (1998).
[10] D.H. Huang, A. Singh, and D.A. Cardimona, J. Appl. Phys. **87**, 2427 (2000).
[11] K.J. Luo, H.T. Grahn, S.W. Teitsworth, and K.H. Ploog, Phys. Rev. B **58**, 12 613 (1998).
[12] D. Sánchez, L. Bonilla, and G. Platero, Phys. Rev. B **63**, 201306 (2001).
[13] D.H. Huang, A. Singh, D.A. Cardimona and C. Morath, J. Appl. Phys. **89**, 4429 (2001).

[14]D.H. Huang, C. Morath, D.A. Cardimona, and A. Singh, J. Appl. Phys. **90**, 6032 (2001).
[15]A. L. Fetter and J. D. Walecka, *Quantum Theory of Many-Particle Systems* (McGraw-Hill, New York, 1971), Chap. 8.
[16]D.A. Cardimona, A. Singh, D.H. Huang, C. Morath, and P. Varangis, Infrared Phys. Technol. **42**, 211 (2001).
[17]D.H. Huang, A. Singh, and D.A. Cardimona, Phys. Lett. A **259**, 488 (1999), and references therein.
[18]K. Flensberg, T.S. Jensen, and N.A. Mortensen, Phys. Rev. B **64**, 245308 (2001).
[19]T. Apostolova, D.H. Huang, P.M. Alsing, J. McIver, and D.A. Cardimona, Phys. Rev. B **66**, 075208 (2002).
[20]B.F. Levine, J. Appl. Phys. **74**, R1 (1993).
[21]D.H. Huang, Phys. Rev. B **53**, 13 645 (1996).
[22]D.H. Huang, G. Gumbs, and M.O. Manasreh, Phys. Rev. B **52**, 14 126 (1995).